POLITECNICO DI TORINO
Repository ISTITUZIONALE

Nonlinear Model Reduction by Moment-Matching for a Point Absorber Wave Energy Conversion System

(Article begins on next page)

17 April 2024

Article

Nonlinear Model Reduction by Moment-Matching for a Point Absorber Wave Energy Conversion System

Guglielmo Papini [1], Francisco Javier Dores Piuma [2], Nicolás Faedo [1,*], John V. Ringwood [3] and Giuliana Mattiazzo [1]

[1] Marine Offshore Renewable Energy Laboratory, Department of Mechanical and Aerospace Engineering, Politecnico di Torino, 10128 Turin, Italy; guglielmo.papini@polito.it (G.P.); giuliana.mattiazzo@polito.it (G.M.)
[2] Departamento de Ciencia y Tecnología, Universidad Nacional de Quilmes, Buenos Aires B1876BXD, Argentina; francisco.dores@alu.unq.edu.ar
[3] Centre for Ocean Energy Research, Maynooth University, W23 F2K8 Kildare, Ireland; john.ringwood@mu.ie
* Correspondence: nicolas.faedo@polito.it

Abstract: This paper presents a data-driven model reduction by moment-matching approach to construct control-oriented models for a point absorber device. The methodology chosen and developed generates models which are input-to-state linear, with any nonlinear behaviour confined to the output map. Such a map is the result of a data-driven approximation procedure, where the so-called moment of the point absorber system is estimated via a least-squares procedure. The resulting control-oriented model can inherently preserve steady-state properties of the target WEC system for a user-defined class of input signals of interest, with the computation only dependent upon a suitably defined set of input-output data.

Keywords: model reduction; moment-matching; wave energy converters; optimal control

1. Introduction

Wave energy converters (WECs) require control algorithms to enhance their efficiency: It is well-established that suitable control system technology, tailored to maximise energy absorption from ocean waves, has the potential to push WEC systems towards effective commercialisation [1–3]. The vast majority of WEC controllers rely upon availability of a suitable control-oriented model, capable of effectively trading accuracy with computational/analytical complexity. The latter can impact both well-posedness of control solutions (i.e., existence of a globally optimal control law for a given operating condition), and real-time capabilities of any specific WEC controller [4]. A pathway towards computation of such parsimonious models is based on model reduction techniques, where a target model is reduced into a 'simpler' (yet representative) structure, with a level of complexity suitable for the specific control task.

The relevance behind incorporating nonlinear effects within the WEC control design procedure, i.e., of using nonlinear control-oriented dynamical models, has been extensively demonstrated and stressed in multiple studies, such as those reported in [5,6]. Wave energy systems are, by design, likely to exhibit substantial nonlinear behaviour, given that their principal objective, pursued by the corresponding optimal control law, is to enhance the device motion in order to maximise energy absorption. This, naturally, challenges the assumptions under which linearisation about the WEC equilibrium position is effectively representative (see, e.g., [5,6]). Though rather scarce, we note that attempts at control-oriented model reduction for WEC systems have been presented in, e.g., [7–10], though simplified models are often computed by selectively 'ignoring' specific nonlinear components, based upon a pre-defined set of operating conditions.

Following the central role of systematic model reduction in producing nonliner control-oriented models for WEC control design procedures, we present, in this manuscript, an ap-

plication of moment-matching-based model reduction wave energy systems. Moment-matching techniques [10–12] have the capability of producing reduced models which effectively matches the steady-state response of the target nonlinear system to be reduced.

In particular, we propose a model reduction approach for a point absorber device (whose geometry and corresponding dimensions are adopted from [13]), based upon data-driven moment-matching [14,15]. This device is an offshore, single body, bottom referenced, floating WEC, which extracts energy from the (translational) heave motion (see Figure 1). The main objective pursued in this paper is that of producing accurate and efficient moment-matching-based reduced models for such a WEC system, subject to a variety of input (wave) conditions. Such objective is achieved by first providing a formal proof on existence and uniqueness of the associated family of reduced order models, and by subsequently employing a fully data-driven algorithm for the approximation of the so-called nonlinear moment, based only on input-output data pairs, being this fundamental towards the final computation of the approximating system. Moreover, the proposed strategy is exhaustively illustrated via numerical analysis.

The reminder of this paper is organised as follows. Section 1.1 presents the notation utilised throughout our study. Section 2 defines the dynamical (target) model of the point absorber system. Section 3 provides a moment-based analysis of the WEC, and proposes a family of reduced models achieving moment-matching from a data-driven perspective. Finally, Section 4 offers a numerical appraisal of the performance of the proposed models, while Section 5 encompasses the main conclusions of our study.
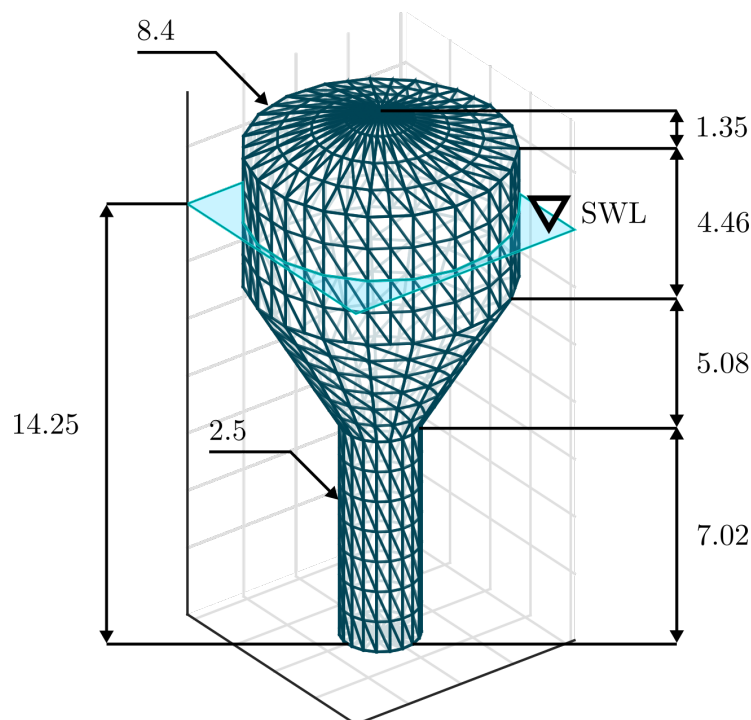
Figure 1. Schematic of the point absorber device under study. Dimensions are presented in metres. Note that the acronym SWL denotes the still water level.

1.1. Notation and Conventions

$\mathbb{R}^+$ is the set of non-negative real numbers, $\mathbb{C}^0$ the set of pure-imaginary complex numbers, and $\mathbb{C}_{<0}$ the set of complex numbers with negative real part. The notation $\mathbb{N}_q$ indicates the set of all positive natural numbers up to q, i.e., $\mathbb{N}_q = \{1, 2, \ldots, q\} \subset \mathbb{N}$. The span of the set $\mathscr{X} = \{x_i\}_{i=1}^k \subset \mathscr{Z}$, where $\mathscr{Z}$ is a vector space over a field $\mathbb{F}$, is denoted as $\text{span}\{\mathscr{X}\}$. The symbol 0 stands for any zero element, dimensioned according to the context. The spectrum of a matrix $A \in \mathbb{R}^{n \times n}$, i.e., the set of its eigenvalues, is

denoted as $\lambda(A)$. Given two functions, $f : \mathscr{Y} \to \mathscr{Z}$ and $g : \mathscr{X} \to \mathscr{Y}$, the composition $(f \circ g)(x) = f(g(x))$, which maps all $x \in \mathscr{X}$ to $f(g(x)) \in \mathscr{Z}$, is denoted with $f \circ g$. Finally, the Fourier transform of a function f (provided it exists), is denoted as $F(\omega)$, $\omega \in \mathbb{R}$.

2. Point Absorber Dynamics

The point absorber WEC device adopted in this study, schematically illustrated in Figure 1, whose geometry and corresponding dimensions are adopted from [13]. The system is essentially an offshore WEC (see [16]), where energy is extracted from the heave (translational) mode of motion. The dimensions of such a (full-scale) device are recalled in the schematic presented in Figure 1.

If we constrain the WEC to move in a single degree-of-freedom [1] (DoF), i.e., heave, the equation of motion of such a device can be expressed as a dynamical system Σ, fully characterised in terms of the the so-called nonlinear Cummins' Equation (see, e.g., [19]), given by [2]

$$\Sigma : \begin{cases} \ddot{z} = \mathcal{M}(f_{rad} + f_e + f_v + f_{re} - u), \\ y = \dot{z}, \end{cases} \tag{1}$$

where $z : \mathbb{R}^+ \to \mathbb{R}$ denotes the displacement of the device (selected as the system output [3] y), $f_{rad} : \mathbb{R}^+ \to \mathbb{R}$ the radiation force (which accounts for the fluid memory effects), $f_v : \mathbb{R}^+ \to \mathbb{R}$ the viscous force, f_{re} the restoring force, $f_e : \mathbb{R}^+ \to \mathbb{R}$, the wave excitation force (i.e., external uncontrollable input representing the force exerted by waves on the surface of the device), $u : \mathbb{R}^+ \to \mathbb{R}$, the control input, and $\mathcal{M} \in \mathbb{R}_{>0}$ is the inverse of the generalised WEC mass.

The radiation force is modelled based on linear potential theory, and can be hence characterised by a linear, continuous-time, strictly proper, passive [4], system Σ_r, which directly depends upon the output of system (1). Without any loss of generality, such an output feedback system can be expressed, in state-space representation, as

$$\Sigma_r : \begin{cases} \dot{\Gamma} = F\Gamma + Gy, \\ f_{rad} = H\Gamma, \end{cases} \tag{2}$$

with $\Gamma(t) \in \mathbb{R}^{n_r}$, with $n_r \in \mathbb{N}_{\geq 1}$ sufficiently large, $F \in \mathbb{R}^{n_r \times n_r}$, and $\{G, H^\mathsf{T}\} \subset \mathbb{R}^{n_r}$. The mapping f_v, characterising viscous effects, is written in terms of a smooth approximation of the so-called Morison Equation [22], i.e.,

$$f_v = -\alpha_v \dot{z} \sqrt{\dot{z}^2 + \epsilon}, \tag{3}$$

with $\epsilon \in \mathbb{R}^+$ sufficiently small, and $\alpha_v \in \mathbb{R}^+$ directly depending on the physical dimensions of the device. The restoring force f_r is expressed in terms of a polynomial mapping in z (see [19]), i.e.,

$$f_{re} = -\beta_{r_0} z + \beta_{r_1} z^2 + \beta_{r_2} z^3, \tag{4}$$

where $\beta_{r_0} \in \mathbb{R}^+$ is commonly referred to as hydrostatic stiffness, and $\{\beta_{r_1}, \beta_{r_2}\} \subset \mathbb{R}$.

With the specific definitions for the mappings offered above, system Σ in (1) can be expressed in state-space form as

$$\Sigma : \begin{cases} \dot{x} = f(x, \zeta) = Ax + B\zeta + g(x), \\ y = h(x) = Cx, \end{cases} \tag{5}$$

with $\zeta = f_e - u$ the total input force, and where the associated state vector is defined as $x = [z \; \dot{z} \; \Gamma^{\mathsf{T}}]^{\mathsf{T}}$, $x(t) \in \mathbb{R}^n$, with $n = 2 + n_r$. The triple of matrices (A, B, C), with $A \in \mathbb{R}^{n \times n}$, $\{B, C^{\mathsf{T}}\} \subset \mathbb{R}^n$, is given by

$$
A = \begin{bmatrix} A^0 & -B^0 H \\ GC^0 & F \end{bmatrix},
$$
$$
B = \begin{bmatrix} B^0 \\ 0 \end{bmatrix},
\tag{6}
$$
$$
C = \begin{bmatrix} C^0 & 0 \end{bmatrix},
$$

together with

$$
A^0 = \begin{bmatrix} 0 & 1 \\ -\mathcal{M}\beta_{r_0} & 0 \end{bmatrix},
$$
$$
B^0 = \begin{bmatrix} 0 \\ \mathcal{M} \end{bmatrix},
\tag{7}
$$
$$
C^0 = \begin{bmatrix} 0 & 1 \end{bmatrix}.
$$

The mapping $g : \mathbb{R}^{2+n_r} \to \mathbb{R}^{2+n_r}$, which is exclusively composed of terms characterising the nonlinear behaviour of system (1), can be written as

$$
g(x) = \begin{bmatrix} g^0(x) \\ 0 \end{bmatrix},
\tag{8}
$$

with g^0 defined as

$$
g^0(x) = \begin{bmatrix} 0 \\ \mathcal{M}\left(-\alpha_v x_2 \sqrt{x_2^2 + \epsilon} + \beta_{r_1} x_1^2 + \beta_{r_2} x_1^3\right) \end{bmatrix}.
\tag{9}
$$

We further note that the maps g and g^0 are such that $g(0) = 0$ and $g^0(0) = 0$ so that, clearly, $f(0,0) = 0$ and $h(0) = 0$.

3. Moment-Based Analysis of the WEC

We present, in this section, the definition of moments for the point absorber device under study, together with an appropriate structure to achieve model reduction by moment-matching. The concepts recalled in this section are based upon the system-theoretic approach originally proposed in [11], later extended to a large class of systems (and inputs) in, e.g., [14,23,24].

From now on, and for aiming to simplify our exposition, we assume the WEC device is subject to regular input excitation f_e with a given fundamental frequency $\omega_0 \in \mathbb{R}^+$. Nonetheless, we do note that extension of the following results to irregular sea states can be conducted analogously to [10] (see also the discussion provided in Remark 2).

Remark 1. *The corresponding optimal control input u, which maximises energy absorption (under state-and-input unconstrained conditions) for such an f_e, is a mapping with the same fundamental frequency ω_0 (see [19,25]).*

3.1. Definition of Moment

In view of Remark 1, let the mapping, corresponding to the total external input $\zeta = f_e - u$, be expressed in implicit form, i.e., in terms of a signal generator (often referred to as an exogenous system), described by the set of equations

$$
\mathcal{G}: \begin{cases} \dot{\xi} = S\xi, \\ \zeta = L\xi, \\ S = \begin{bmatrix} 0 & \omega_0 \\ -\omega_0 & 0 \end{bmatrix}, \end{cases}
\tag{10}
$$

for $t \in \mathbb{R}^+$, with $\{\xi(t), L^\mathsf{T}\} \subset \mathbb{R}^\nu$, and hence $S \in \mathbb{R}^{\nu \times \nu}$, with $\nu = 2$. From now on, and without any loss of generality, let the output vector of $\mathcal{G}$ be defined as $L = [1\ 1]$.

Remark 2. *As discussed previously in this section, and for simplicity of exposition, the signal generator in* (10) *considers that the corresponding system input is composed of a single fundamental frequency component ω_0, i.e., the device is subject to regular (monochromatic) waves. Extension of this strategy for irregular sea states can be performed analogously to the model-based reduction framework in [10], by defining a corresponding signal generator with a sufficiently large set of harmonic multiples of ω_0, i.e., with a dynamic matrix S_e given by*

$$
S_e = \bigoplus_{p=1}^{d} \begin{bmatrix} 0 & h_p \omega_0 \\ -h_p \omega_0 & 0 \end{bmatrix}
\tag{11}
$$

with the set of harmonic frequencies $\mathscr{F} = \{h_p \omega_0\}_{p=1}^{d} \subset \mathbb{R}^+$, where $\mathcal{H} = \{h_p\} \subset \mathbb{N}_{\geq 1}$, and adapting the upcoming results accordingly.

We now introduce the following standing assumption, adopted from [23,23].

Assumption 1. *The pair of matrices $(S, \xi(0))$ is excitable.*

Remark 3. *For linear systems, excitability is equivalent to reachability, with $x(0)$ playing the role of the input matrix* [5].

Remark 4. *If $(S, \xi(0))$ is excitable, i.e., under Assumption 1, one can easily check that $span\{\xi_1, \xi_2\} = span\{\cos(\omega_0 t), \sin(\omega_0 t)\}$, and hence the input mapping ζ is T_0-periodic, where $T_0 = 2\pi/\omega_0 \in \mathbb{R}^+$ the fundamental period of ζ.*

Aiming to provide a formal definition of moment for the point absorber device described in Equation (5), we further introduce an assumption regarding the stability of Σ. Note that, due to the nature of the nonlinear map g, defined in Equation (8), one can check that $(x, \zeta) = (0, 0)$ is an equilibrium (invariant) point of the system defined in Equation (5) straightforwardly, i.e., $\partial g / \partial x|_{(x,\zeta)=(0,0)} = 0$.

Assumption 2. *The zero equilibrium of the point absorber system $\dot{x} = f(x, 0)$ is locally exponentially stable.*

Note that Assumption 2 is without any loss of generality since, for any set of physically meaningful parameters, system (5) is such that $\lambda(A) \subset \mathbb{C}_{<0}$, and hence the zero-equilibrium of $\dot{x} = f(x, 0)$ is locally exponentially stable (see [13,19]). We are now ready to introduce our first proposition, based upon fundamental results presented in [11].

Proposition 1. *Consider the point absorber system* (5) *with an input mapping ζ described in terms of the signal generator* (10). *Let L* = [1 1]. *If Assumptions 1 and 2 hold, there exists a map π, locally defined in a neighbourhood Ξ of ξ* = 0, *with π*(0) = 0, *which solves:*

$$\frac{\partial \pi(\xi)}{\partial \xi} S\xi = f(\pi(\xi), L\xi),$$

(12)

for all ξ ∈ Ξ, *and the steady-state response of the interconnected system* (5)–(10) *is* $x_{\mathrm{ss}}(t) = \pi(\xi(t))$, *for any x*(0) *and ξ*(0) *sufficiently small.*

Proof. See Appendix A for a proof of this statement. □

Definition 1 ([11]). *The mapping h ∘ π is the moment of the point absorber system* (5) *at the signal generator* (10), *i.e., at* $\mathcal{G}$.

Remark 5. *The notion of moment in Definition 1, together with the result offered in Proposition 1, imply that the moment of the point absorber WEC system defined in Equation* (5) *at the signal generator* $\mathcal{G}$, *computed along a particular trajectory ξ*(t), *coincides with the (well-defined) steady-state response of the output of the interconnected system* (5)–(10), *i.e.,* $y_{ss}(t) = h(\pi(\xi(t)))$.

3.2. Model Reduction by Moment-Matching

As briefly discussed throughout Section 1, the theoretical grounds underlying model reduction by moment-matching are rooted in the strong existing connection between moments, as mathematical objects (see Definition 1), and the steady-state output response of the composite system (5)–(10) (see, e.g., [11]). Aiming to keep this paper reasonably self-contained, we recall the definition of a moment-based reduced order model for the nonlinear point absorber WEC system (5), driven by the class of inputs generated by (10).

Definition 2 ([11]). *Consider the point absorber system Σ in* (5) *and the autonomous system defined in* (10). *The dynamical system*

$$\tilde{\Sigma} : \begin{cases} \dot{\Omega} = \varrho(\Omega, \zeta), \\ \tilde{y} = \sigma(\Omega), \end{cases}$$

(13)

with ϱ : $\mathbb{R}^\nu \times \mathbb{R} \to \mathbb{R}^\nu$, *σ* : $\mathbb{R}^\nu \to \mathbb{R}$, $\Omega(t) \in \mathbb{R}^\nu$, *and* $\tilde{y}(t) \in \mathbb{R}$, *is called a model of system* (5) *at the signal generator* $\mathcal{G}$, *if system* (13) *has the same moments at* $\mathcal{G}$ *as system* (5). *Furthermore, if ν* < *n, we call system* (13) *a reduced order model of system* (5) *at* $\mathcal{G}$.

Though Definition 2 formally introduces the concept of a model reduced by moment-matching, its actual computation is still implicit. Following the result presented in [12], a particularly simple family of reduced models, achieving moment-matching at $\mathcal{G}$, of order (dimension) ν = 2, for the point absorber device defined in equation (5), can be explicitly written in terms of the mapping *h ∘ π*, with π the solution of (12), as

$$\tilde{\Sigma} : \begin{cases} \dot{\Omega} = (S - \Delta L)\Omega + \Delta \zeta, \\ \tilde{y} = h(\pi(\Omega)), \end{cases}$$

(14)

with Δ ∈ $\mathbb{R}^2$ a free (design) parameter.

Remark 6. *Equation* (14) *defines a family of reduced order models achieving moment-matching described by an input-to-state linear differential equation with a nonlinear output map. Note that this is highly appealing from a computational perspective: the main 'cost' behind solving* (14) *for a given input signal is merely the cost of solving a linear operator. This is further demonstrated in Section 4 by means of numerical analysis.*

Remark 7. *Note that, if $\lambda(S - \Delta L) \subset \mathbb{C}_{<0}$, the family of models (14) has the exact same steady-state output response of the nonlinear target point absorber WEC system Σ at the signal generator $\mathcal{G}$. Furthermore, given the observability condition on the pair (S, L), the complex-valued set $\lambda(S - \Delta L)$ can be freely assigned. This, naturally, allows for preservation of particular properties of the target system to be reduced in the computed simplified structure.*

Remark 8. *The success of the family of systems (14) in practical scenarios depends entirely upon the mapping $h \circ \pi$, i.e., the corresponding moment, which solves the partial differential equation (12). Given that, in practice, this is far from trivial (even when in possession of exact knowledge of the system dynamics defined by f and h in (5)), a data-driven formulation is adopted in Section 3.3, to approximate the corresponding moment based upon input-output data.*

We now introduce the following result, which is analogous to (Lemma 4, [15]). In particular, we show that the moment for the point absorber device, computed along a specific trajectory of (10), is T_0-periodic, with $T_0 = 2\pi/\omega_0$. This result is instrumental to the data-driven approach presented in Section 3.3.

Proposition 2. *Let $L = [1\ 1]$ and suppose Assumptions 1 and 2 hold. Then, the mapping $h \circ \pi \circ \xi$ is T_0-periodic.*

Proof. See Appendix B for a proof of this statement. □

3.3. Approximation of $h \circ \pi$

Motivated by the discussion provided in Remark 8, we follow a data-driven approach to compute an approximation of the corresponding moment. Such a framework was originally introduced in [14], and extended to a specific class of WEC systems in [15]. To achieve a consistent approximation for $h \circ \pi$, we begin by introducing the following assumption.

Assumption 3. *The mapping $h \circ \pi$ belongs to the space generated by a family of continuous real-valued functions $\{\chi_j\}_{j=1}^{\infty}$, with $\chi_i : \mathbb{R}^2 \to \mathbb{R}$, i.e., there exists a set of constants v_j such that $(h \circ \pi)(\xi) = \sum_{j=1}^{\infty} v_j \chi_j(\xi)$, for every $\xi \in \Xi$.*

Assumption 3 facilitates an almost natural definition for an approximation of $h \circ \pi$, as detailed in the following.

Definition 3. *We call the mapping $\widetilde{(h \circ \pi)}(\xi) = \sum_{j=1}^{N} v_j \chi_j(\xi)$, with N finite, the approximated moment of the point absorber system (5) at the signal generator $\mathcal{G}$.*

Remark 9. *When choosing the set of functions $\{\chi_j\}$, the user can proceed in a 'trial and error' procedure, depending on the specific nature of the WEC dynamics. In this paper, we show that a polynomial expansion can be effectively used to approximate the associated moment for the point absorber studied (see Section 4).*

Based upon Definition 3, the data-driven approach adopted in our study aims to compute the set of coefficients $\{v_j\}_{j=1}^{N}$ for the point absorber WEC case, by using information on the steady-state output response of (5). Let us define:

$$\begin{aligned} \mathrm{Y} &= \begin{bmatrix} v_1 & v_2 & \ldots & v_N \end{bmatrix}, \\ X(\xi) &= \begin{bmatrix} \chi_1(\xi) & \chi_2(\xi) & \cdots & \chi_N(\xi) \end{bmatrix}^{\mathsf{T}}, \end{aligned} \tag{15}$$

where $\{\mathrm{Y}^{\mathsf{T}}, X(\xi)\} \subset \mathbb{R}^N$, and hence the approximated moment can be expressed as

$$\widetilde{(h \circ \pi)}(\xi) = \mathrm{Y}X(\xi). \tag{16}$$

Let $\{\xi^i(t)\}_{i=1}^P \subset \mathbb{R}^2$ be a set of trajectories for the signal generator $\mathcal{G}$ in (10), computed via a set of corresponding initial conditions $\{\xi(0)^i\}_{i=1}^P \subset \mathbb{R}^2$, such that each element in the set $\{(S, \xi(0)^i)\}_{i=1}^P$ is excitable, i.e., Assumption 1 holds. Let $\{y_{ss}^i(t)\}_{i=1}^P \subset \mathbb{R}$ denote the set of steady-state outputs (computed after a sufficiently large time T_{ss}) of the point absorber system (5), driven by each generated input $\zeta^i(t) = [1\,1]\xi^i(t)$.

Based upon the sets defined immediately above, and since the (well-defined) steady-state output response of Σ in (5) coincides with the associated moment $h \circ \pi$ evaluated at the corresponding trajectory of the signal generator (10) (see Proposition 1), the approximation $\widetilde{h \circ \pi}$ can be computed as follows. Let $\mathcal{T} = \{t_q\}_{q=1}^R \subset [T_{ss}, T_{ss} + T_0]$, where each t_q represents a time instant, with $R > P$. Define $\{\mathcal{M}_i\}_{i=1}^P \subset \mathbb{R}^{N \times R}$ and $\{\mathcal{O}_i^\mathsf{T}\}_{i=1}^P \subset \mathbb{R}^R$ such that

$$\begin{aligned}
\mathcal{M}_i &= \begin{bmatrix} X(\xi^i(t_1)) & X(\xi^i(t_2)) & \dots & X(\xi^i(t_R)) \end{bmatrix}, \\
\mathcal{O}_i &= \begin{bmatrix} y_{ss}^i(t_1) & y_{ss}^i(t_2) & \dots & y_{ss}^i(t_R) \end{bmatrix},
\end{aligned} \tag{17}$$

and hence

$$\begin{aligned}
\mathcal{M} &= \begin{bmatrix} \mathcal{M}_1 & \mathcal{M}_2 & \dots & \mathcal{M}_P \end{bmatrix}, \\
\mathcal{O} &= \begin{bmatrix} \mathcal{O}_1 & \mathcal{O}_2 & \dots & \mathcal{O}_P \end{bmatrix}.
\end{aligned} \tag{18}$$

Before proceeding with the actual computation of $\widetilde{h \circ \pi}$, we introduce one last standing assumption.

Assumption 4. *The set of time-instants $\mathcal{T}$ is chosen such that $\mathcal{M}$ in (18) is full row rank.*

Remark 10. *Given the signal generator (10), and the excitability condition guaranteed by Assumption 1, Assumption 4 is without any loss of generality, since the set $\mathcal{T}$ can always be chosen such as $\mathcal{M}$ in (18) has rank N (see [14,26]).*

Finally, note that the coefficient matrix Y, characterising the approximated moment $\widetilde{h \circ \pi}$ (see Equation (16)), can be uniquely computed in terms of the least-squares solution of $Y\mathcal{M} = \mathcal{O}$, i.e.,

$$Y = \mathcal{O}\mathcal{M}^\mathsf{T}(\mathcal{M}\mathcal{M}^\mathsf{T})^{-1}, \tag{19}$$

where the condition $0 \notin \lambda(\mathcal{M}\mathcal{M}^\mathsf{T})$ is always guaranteed by Assumption 4.

Remark 11. *The least-squares solution proposed in (19) is effectively exploiting the result of Proposition 2. In particular, given that $h(\pi(\xi(t)))$ is T_0-periodic, it is sufficient to use the information of the steady-state output response of the point absorber system (5) over a single period, i.e., $[T_{ss}, T_{ss} + T_0]$, to fully characterise $h(\pi(\xi(t)))$.*

Remark 12. *Note that, while we explicitly use the (analytical) definition of system (5) throughout our paper, the set of steady-state output data $\{y_{ss}^i\}$ can be generated either with a different numerical model (e.g., solvers based upon computational fluid dynamics), or collected from tailored experiments involving a real WEC prototype.*

3.4. Systematic Overview

We provide, in this subsection, a systematic overview of the proposed model reduction procedure, defining a number of fundamental steps ($S_\#$) towards the computation of a reduced model by moment-matching for WEC systems, based upon the results presented throughout Section 3. In addition, we provide a companion schematic illustration of the procedure described in this section, in Figure 2.

(S_1)　Choose the fundamental frequency $\omega_0 = 2\pi/T_0$ associated with the selected wave conditions.

(S_2)　Compute S as in Equation (10) and set $L = [1\ 1]$.

(S_3)　Compute the set of trial trajectories $\{\xi^i(t)\}_{i=1}^P$ via the set of initial conditions $\{\xi^i(0)\}_{i=1}^P$ of interest.

(S_4)　Compute the set of associated input signals $\{\zeta^i(t) = L\xi^i(t)\}_{i=1}^P$.

(S_5)　For each defined input ζ^i, with $i \in \mathbb{N}_P$, compute the steady-state output response of the WEC system $\{y_{ss}^i(t)\}_{i=1}^P$ (collected after a sufficiently large time T_{ss}).

(S_6)　Choose the set of time instants $\mathcal{T} = \{t_q\}_{q=1}^R$, with $R > P$, such that $\mathcal{T} \subset [T_{ss}, T_{ss} + T_0]$ and Assumption 4 holds.

(S_7)　Compute the matrices $\mathscr{M}$ and $\mathscr{O}$ as in Equation (18).

(S_8)　Compute Y as the unique least-square solution expressed in (19).

(S_9)　Construct the family of reduced order models achieving moment-matching for the WEC system as

$$\tilde{\Sigma} : \begin{cases} \dot{\Omega} = (S - \Delta L)\Omega + \Delta\zeta, \\ \tilde{y} = CYX(\Omega) \approx y, \end{cases}$$

for any matrix Δ such that $\lambda(S - \Delta L) \subset \mathbb{C}_{<0}$.
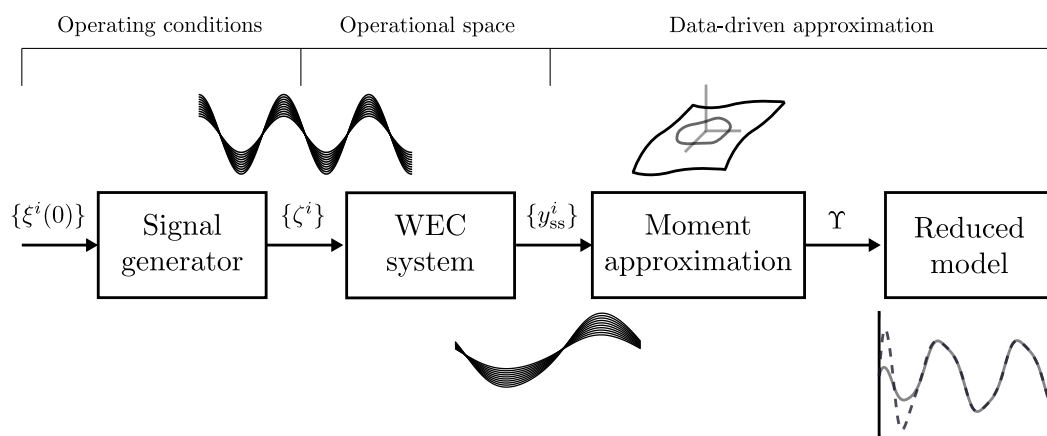
Figure 2. Schematic representation of the model reduction by moment-matching procedure described throughout Section 3.

4. Numerical Study

For the numerical study presented in this section, we consider the point absorber device described by the dynamical model presented in Section 2, and schematically illustrated in Figure 1. The numerical values for the set of parameters, corresponding with the target system Σ in (5), are as adopted in [19]. The characterisation of the radiation subsystem in (2) is performed here via boundary element methods, using the open-source software NEMOH [27], in combination with a moment-based finite-order parametrisation procedure [28,29], rendering a model Σ_r with order $n_r = 6$.

To illustrate the nature of the nonlinear behaviour of the device under scrutiny, i.e., the characteristics of the map g in Equation (8), Figure 3 shows the 'magnitude' of the associated nonlinear effects (measured in terms of the 2-norm $\|g(x)\|$), as a function of the first two state variables x_1 (displacement, in metres), and x_2 (velocity, in metres per second). It can be readily appreciated that, as soon as the device moves away from the physical equilibrium position $(x_1, x_2) = (0, 0)$, $\|g(x)\|$ grows rapidly, stressing the relevance of the associated nonlinear effects as soon as the WEC system departs from 'small motion' conditions.
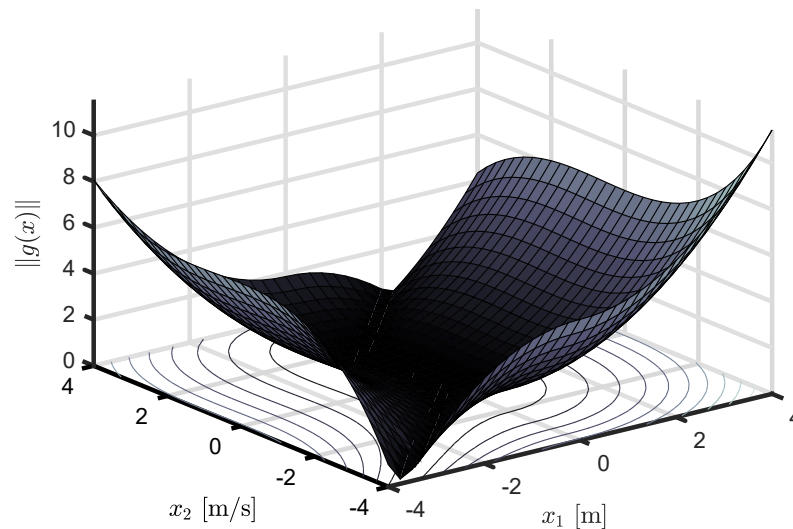
Figure 3. Indicative measure of the nonlinear behaviour associated with the point absorber system under study.

Recall that, to construct the corresponding reduced order model, a data-driven approximation method is considered in Section 3.3. In particular, such a method explicitly uses input–output data to reconstruct an approximation of moment associated with the point absorber system (5). In line with Section 3.3, Figure 4 presents the set of inputs $\zeta^i(t)$, $i \in \mathbb{N}_{10}$, constructed via different initial conditions for the signal generator (10), used to excite system Σ, with a fundamental frequency $\omega_0 \approx 1$ [rad/s]. Note that such a set of signals corresponds to a controlled WEC operating in regular sea states with period $T_0 \approx 6$ [s], and wave heights in the set $[0.5, 3]$ [m]. With the set of inputs illustrated in Figure 4, we compute the corresponding set of steady-state outputs for the target system (5). These are presented, using a solid-black line, in Figure 5.
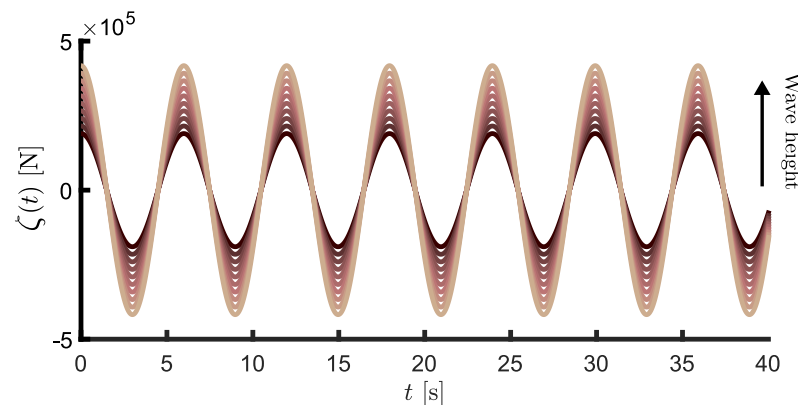

Figure 4. Set of inputs ζ^i used to approximate the associated moment.

For the selection of the function space generated by the set $\{\chi_i\}_{i=1}^N$, used to approximate the corresponding moment (see Definition 3), we select a smooth (polynomial) mapping, defining a (ξ_1, ξ_2) manifold, i.e.,

$$\widetilde{(h \circ \pi)}(\xi) = \sum_{i=0}^{4} \sum_{j=0}^{3} v_{ij} \xi_1^i \xi_2^j, \tag{20}$$

where $N = 20$. Having defined the corresponding input–output set, and the approximation structure of (20), we can directly apply the methodology presented in Section 3.3, and compute the corresponding approximated moment via the well-defined least-squares solution in (19). The optimal coefficients corresponding to the expansion in (20) are presented here

in Figure 6, while the outputs resulting from evaluating the approximated moment at each corresponding trajectory of the signal generator (10) are presented in Figure 5, using a dashed-red line, showing a virtually perfect match with each target. Note that, as per the procedure proposed throughout Section 3, a single period $T_0 \approx 6$ [s] is shown in Figure 5, which is sufficient to fully characterise the T_0-periodic steady-state output response of the WEC system.
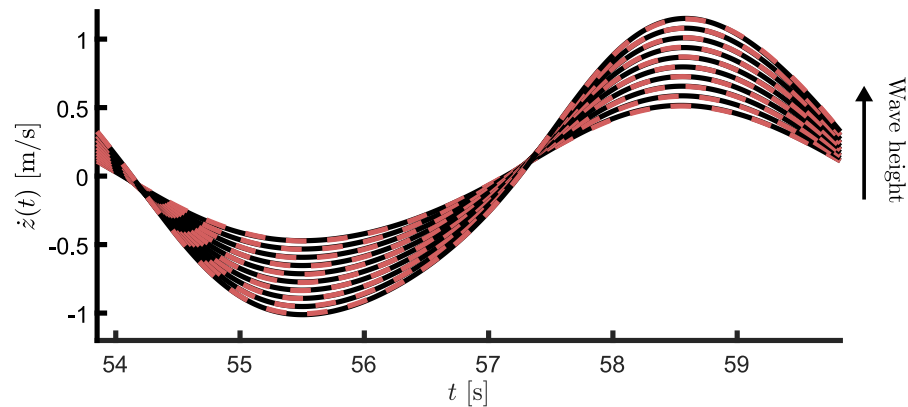

Figure 5. Target steady-state responses (solid-black), along with the data-driven approximating moment evaluated at each specific trajectory of $\mathcal{G}$ (dashed-red).
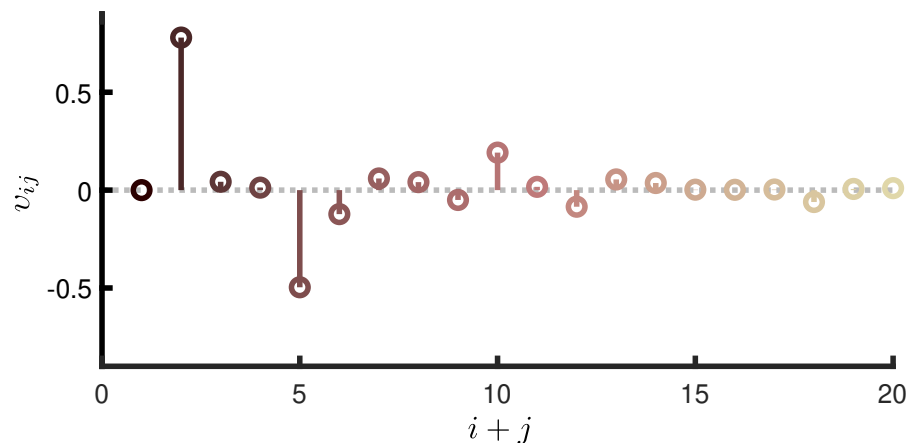
Figure 6. Computed coefficients ε_{ij} for the polynomial expansion (20).

Remark 13. *Note that the absolute value of some of the coefficients presented in Figure 6 are very close to zero, hence suggesting we could directly prescind of such a set in (20).*

The approximation results presented in Figure 5 are extended in Figure 7, where the approximated manifold (20) can be effectively appreciated, together with the target moment evaluated at each trajectory $\xi(t)$ corresponding with the set of inputs of Figure 4. Note that we also include the corresponding planar projections for each triple $(\xi_1(t), \xi_2(t), h(\pi(\xi(t))))$.
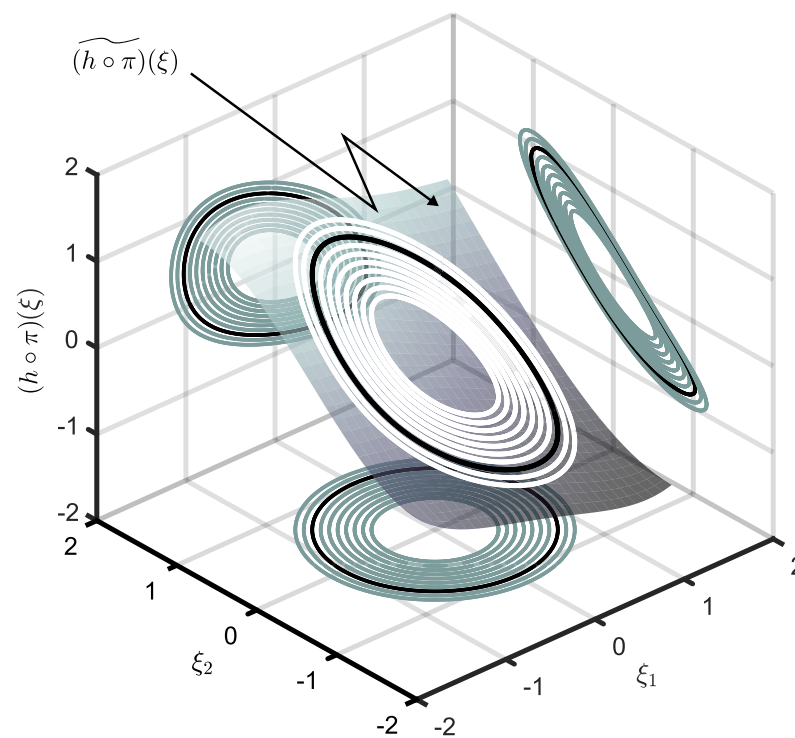
**Figure 7.** Approximated moment $\widetilde{(h \circ \pi)}(\xi)$.

Up until this point, we have presented results concerning the approximation of the moment of the point absorber system. We now use such results to build a reduced model, which is effectively the ultimate objective of this study. Based upon the structure presented in (14), we can construct a 2nd order reduced model for the point absorber system (5) simply as

$$\tilde{\Sigma} : \begin{cases} \dot{\Omega} = \left(\begin{bmatrix} 0 & -0.6 \\ 0.6 & 0 \end{bmatrix} - \Delta \begin{bmatrix} 1 & 1 \end{bmatrix} \right) \Omega + \Delta \zeta, \\ \tilde{y} = \widetilde{(h \circ \pi)}(\Omega), \end{cases} \tag{21}$$

with a gain matrix Δ chosen such that the set $\lambda(S - \Delta L) = \{-0.13 \pm j2.04\}$, which coincides with the set of two dominant modes of the Jacobian linearisation of the WEC system about the equilibrium position. Aiming to illustrate the nature of the resulting linear input-to-state dynamics in (21), Figure 8 presents a Bode plot of both the Jacobian linearisation of the point absorber model (5) (dotted-blue), and the corresponding linearisation of the reduced model (21) (dashed-red). Note that the latter can be readily defined in terms of (20) as

$$\tilde{\Sigma}_l : \begin{cases} \dot{\Omega} = \left(\begin{bmatrix} 0 & -0.6 \\ 0.6 & 0 \end{bmatrix} - \Delta \begin{bmatrix} 1 & 1 \end{bmatrix} \right) \Omega + \Delta \zeta, \\ \tilde{y}_l = \begin{bmatrix} v_{10} & v_{01} \end{bmatrix} \Omega. \end{cases} \tag{22}$$

It is clear from Figure 8 that, besides being capable of representing the nonlinear behaviour of the associated WEC system (see also the discussion provided in the following paragraph), the computed reduced model by moment-matching is also able to preserve the dynamics of the WEC system in linear operating conditions. Furthermore, as can be appreciated from Figure 9, the Nyquist plot of system (22) is fully defined on the right-hand-side of the complex plane, i.e., the nonlinear reduced model (21) is locally passive (see, e.g., [30]). Fulfilment of this property not only highlights the consistency of the reduced model with respect to the underlying physical reality of the WEC energy absorption process, but is also fundamental to guarantee existence and uniqueness (i.e., well-possedness) of the solution of a vast family of WEC optimal control algorithms [31].
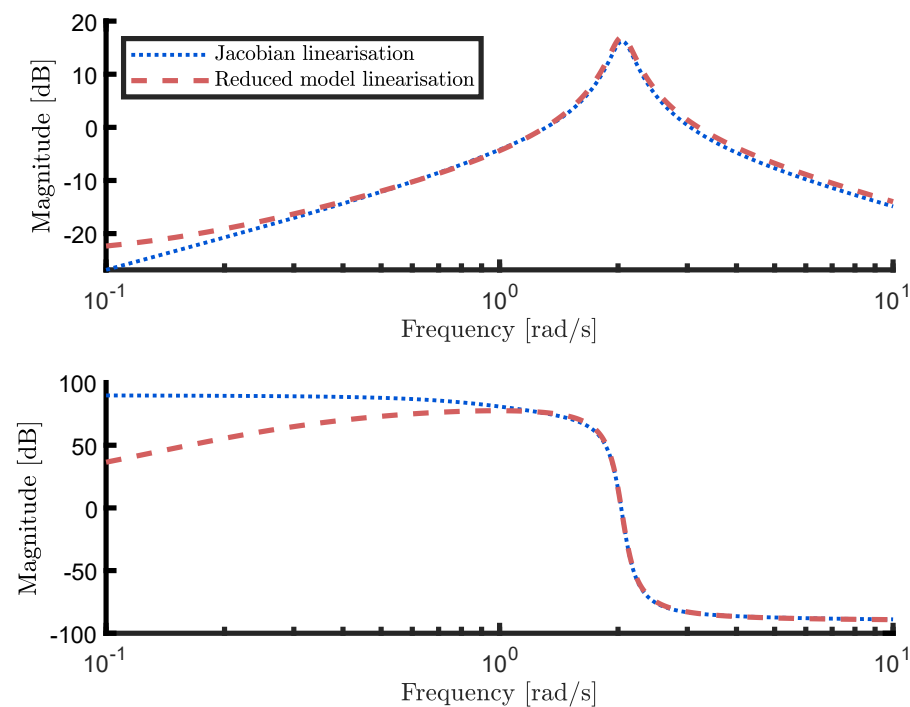
Figure 8. Bode plot of the Jacobian linearisation of the WEC dynamical Equation (5) (dotted-blue), and that associated with the reduced model, i.e., Equation (22).
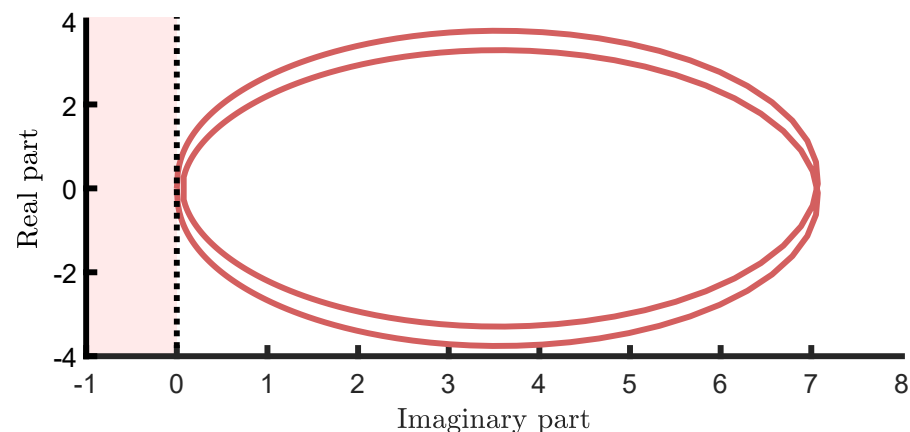

Figure 9. Nyquist plot of system (22).

Aiming at illustrating the accuracy of the computed reduced model (21) under nonlinear operating conditions, Figure 10 (top) shows output time-traces for both the target nonlinear (solid-black) point absorber system (5), and the moment-based reduced order model (dashed-red) model (21), for an input ζ corresponding to a wave height of 2.5 [m]. Furthermore, Figure 10 (bottom) offers the evolution of the absolute value of the approximation error, i.e., $|y - \tilde{y}|$. It is hence straightforward to appreciate that, once the transient period extinguishes, target and approximating time traces become almost indistinguishable, as expected from the moment-matching-based model reduction procedure proposed in Section 3. Finally, Figure 11 offers a comparison between the normalised run-time [6] required by both target (solved via a Runge–Kutta (4,5) pair), and reduced model by moment-matching. It is clear that the reduced model computes in an order of magnitude faster than the target nonlinear WEC system, both due to its smaller order (dimension), and its linear input-to-state nature.
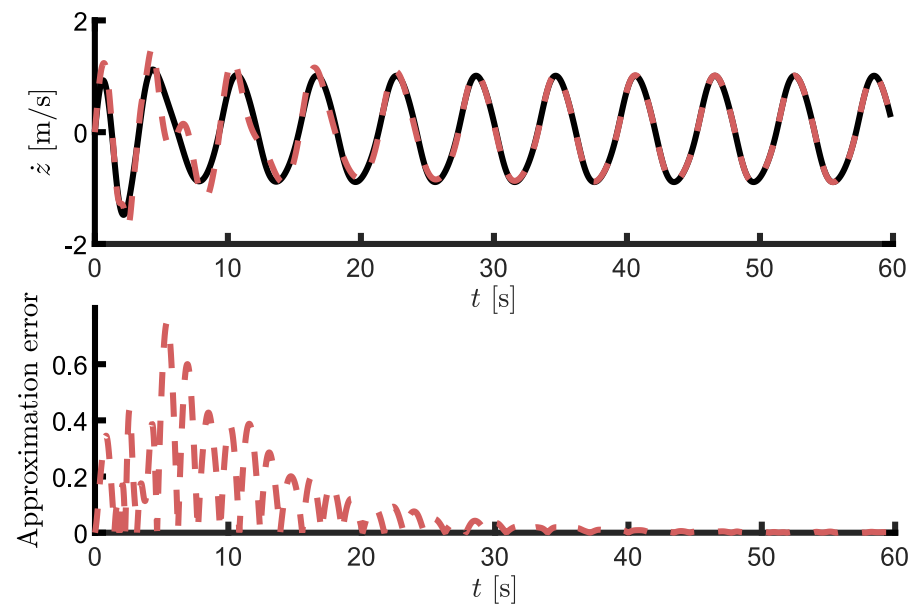
Figure 10. (**Top**): Output traces for target point absorber system (solid-black), and the computed approximating model by moment-matching (dashed-red). (**Bottom**): Error between target and approximating response as a function of time.
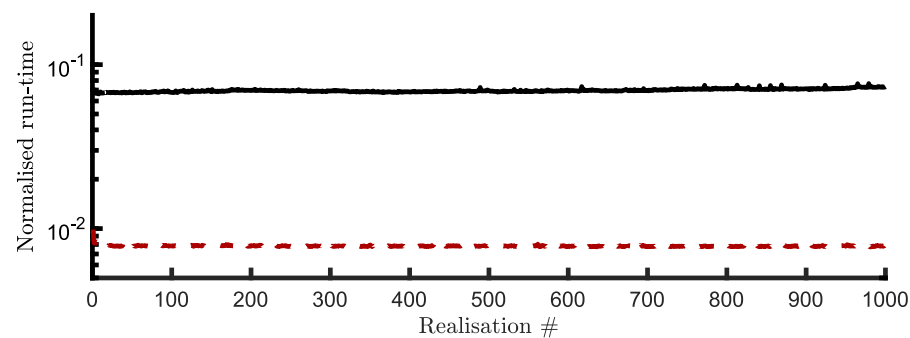
Figure 11. Normalised run-time required to solve the target nonlinear WEC model (solid black), and the reduced model by moment-matching (dashed red).

5. Conclusions

This paper presents a data-driven approach to construct reduced models for a state-of-the-art wave energy conversion system. The methodology chosen and developed generates models which are input-to-state linear, with any nonlinear behaviour confined to the output map. Such a map is the result of a data-driven approximation procedure, where the so-called moment of the point absorber system is estimated via a least-squares procedure. The user has full control over the complexity of such an approximation, being able to freely select the characteristics of the associated approximation space. The performance of the strategy is illustrated via a numerical case study, showing that the approach is capable of providing parsimonious models with preservation of steady-state response characteristics.

Institutional Review Board Statement: Not applicable.

Informed Consent Statement: Not applicable.

Conflicts of Interest: The authors declare no conflicts of interest. The funders had no role in the design of the study; in the collection, analyses, or interpretation of data; in the writing of the manuscript; or in the decision to publish the results.

Appendix A. Proof of Proposition 1

We begin by noting that, under Assumption 1, the triple of matrices $(L, S, \xi(0))$ is effectively minimal. Furthermore, note that the signal generator (10) is such that $\lambda(S) \subset \mathbb{C}^0$ with corresponding eigenspaces $\{\mathscr{A}_1, \mathscr{A}_2\}$ such that $\dim(\mathscr{A}_i) = 1$ for $i \in \{1, 2\}$, i.e., the generator $\mathcal{G}$ is Poisson stable. Under these conditions, the result of this proposition holds directly via [11], as long as the zero equilibrium of the point absorber system $\dot{x} = f(x, 0)$ is locally exponentially stable. Since this is the case by Assumption 2, the proof follows.

Appendix B. Proof of Proposition 2

The definition of the autonomous system (10) directly implies that the function ζ is T_0-periodic, with a period $T_0 = 2\pi/\omega_0$ (see Remark 4). Furthermore, by Assumption 2, the zero equilibrium of (5) is locally exponentially stable, and its (well-defined) steady-state solution is also T_0-periodic (the reader is referred to [32] for further detail). Taking into account the minimality condition on the triple $([1\,1], S, \xi(0))$, i.e., Assumption 1, the following equality $x_{\mathrm{ss}}(t) = \pi(\xi(t))$ holds (see Proposition 1), and it is hence we can conclude that $h \circ \pi \circ \xi$ is T_0-periodic.

Notes

1. Note that this is performed without any loss of generality, and aiming to simplify the notation used throughout our study. Similar considerations can be made for a multi-DoF WEC system (see, e.g., [17,18].)
2. From now on, the dependence on t is dropped when clear from the context.
3. Note that this is performed without any loss of generality, and merely due to the importance of the velocity variable within the WEC optimal control formulation.
4. See [20,21] for a formal discussion on the dynamical properties associated with Σ_r.
5. The interested reader is referred to [26] for a formal treatment of the concept of excitability for a general class of systems.
6. The normalised run-time is defined as the time required to compute the output corresponding to each analysed model, and the simulation length.

References

1. Ringwood, J.V. Wave energy control: Status and perspectives 2020. *IFAC-PapersOnLine* **2020**, *53*, 12271–12282. [CrossRef]
2. Ringwood, J.V.; Bacelli, G.; Fusco, F. Energy-maximizing control of wave-energy converters: The development of control system technology to optimize their operation. *IEEE Control Syst.* **2014**, *34*, 30–55.
3. García-Violini, D.; Faedo, N.; Jaramillo-Lopez, F.; Ringwood, J.V. Simple Controllers for Wave Energy Devices Compared. *J. Mar. Sci. Eng.* **2020**, *8*, 793. [CrossRef]
4. Faedo, N. Optimal Control and Model Reduction for Wave Energy Systems: A Moment-Based Approach. Ph.D. Thesis, National University of Ireland, Maynooth, Ireland, 2020.
5. Giorgi, G.; Gomes, R.P.F.; Bracco, G.; Mattiazzo, G. Numerical investigation of parametric resonance due to hydrodynamic coupling in a realistic wave energy converter. *Nonlinear Dyn.* **2020**, *101*, 153–170. [CrossRef] [PubMed]
6. Giorgi, G. Nonlinear Hydrodynamic Modelling of Wave Energy Converters under Controlled Conditions. Ph.D. Thesis, Department of Electronic Engineering, Maynooth University, Maynooth, Ireland, 2018.
7. Suchithra, R.; Ezhilsabareesh, K.; Samad, A. Development of a reduced order wave to wire model of an OWC wave energy converter for control system analysis. *Ocean Eng.* **2019**, *172*, 614–628. [CrossRef]
8. Penalba Retes, M.; Ringwood, J.V. Systematic complexity reduction of wave-to-wire models for wave energy system design. *Ocean Eng.* **2020**, *217*, 107651. [CrossRef]
9. Penalba, M.; Ringwood, J.V. Linearisation-based nonlinearity measures for wave-to-wire models in wave energy. *Ocean Eng.* **2019**, *171*, 496–504. [CrossRef]
10. Faedo, N.; Piuma, F.J.D.; Giorgi, G.; Ringwood, J.V. Nonlinear model reduction for wave energy systems: A moment-matching-based approach. *Nonlinear Dyn.* **2020**, *102*, 1215–1237. [CrossRef]

11. Astolfi, A. Model reduction by moment matching for linear and nonlinear systems. *IEEE Trans. Autom. Control* **2010**, *55*, 2321–2336. [CrossRef]

12. Scarciotti, G.; Astolfi, A. Nonlinear Model Reduction by Moment Matching. *Found. Trends Syst. Control* **2017**, *4*, 224–409. [CrossRef]

13. Hals, J.; Ásgeirsson, G.S.; Hjálmarsson, E.; Maillet, J.; Möller, P.; Pires, P.; Guérinel, M.; Lopes, M. Tank testing of an inherently phase-controlled wave energy converter. *Int. J. Mar. Energy* **2016**, *15*, 68–84.

14. Scarciotti, G.; Astolfi, A. Data-driven model reduction by moment matching for linear and nonlinear systems. *Automatica* **2017**, *79*, 340–351. [CrossRef]

15. Faedo, N.; Piuma, F.J.D.; Giorgi, G.; Bracco, G.; Ringwood, J.V.; Mattiazzo, G. Data-driven nonlinear model reduction by moment-matching for the ISWEC system. In Proceedings of the 2021 International Conference on Electrical, Computer, Communications and Mechatronics Engineering (ICECCME), Mauritius, Mauritius, 7–8 October 2021; pp. 1–6.

16. Korde, U.A.; Ringwood, J.V. *Hydrodynamic Control of Wave Energy Devices*; Cambridge University Press: Cambridge, UK, 2016.

17. Folley, M.; Forehand, D. Chapter 8—Conventional Multiple Degree-of-Freedom Array Models. In *Numerical Modelling of Wave Energy Converters*; Folley, M., Ed.; Academic Press: New York, NY, USA, 2016; pp. 151–164.

18. Faedo, N.; Scarciotti, G.; Astolfi, A.; Ringwood, J.V. Energy-maximising moment-based constrained optimal control of ocean wave energy farms. *IET Renew. Power Gener.* **2021**, *15*, 3395–3408. [CrossRef]

19. Faedo, N.; Scarciotti, G.; Astolfi, A.; Ringwood, J.V. Nonlinear energy-maximizing optimal control of wave energy systems: A moment-based approach. *IEEE Trans. Control Syst. Technol.* **2021**, *29*, 2533–2547. [CrossRef]

20. Faedo, N.; Peña-Sanchez, Y.; Ringwood, J.V. Parametric representation of arrays of wave energy converters for motion simulation and unknown input estimation: A moment-based approach. *Appl. Ocean Res.* **2020**, *98*, 102055. [CrossRef]

21. Pérez, T.; Fossen, T.I. Time-vs. frequency-domain identification of parametric radiation force models for marine structures at zero speed. *Model. Identif. Control* **2008**, *29*, 1–19. [CrossRef]

22. Morison, J.; Johnson, J.; Schaaf, S.A. The force exerted by surface waves on piles. *J. Pet. Technol.* **1950**, *2*, 149–154. [CrossRef]

23. Astolfi, A.; Scarciotti, G.; Simard, J.; Faedo, N.; Ringwood, J.V. Model Reduction by Moment Matching: Beyond Linearity A Review of the Last 10 Years. In Proceedings of the 2020 59th IEEE Conference on Decision and Control (CDC), Jeju, Korea, 14–18 December 2020; pp. 1–16.

24. Faedo, N.; Scarciotti, G.; Astolfi, A.; Ringwood, J.V. On the Approximation of Moments for Nonlinear Systems. *IEEE Trans. Autom. Control* **2021**, *66*, 5538–5545. [CrossRef]

25. Faedo, N.; Carapellese, F.; Pasta, E.; Mattiazzo, G. On the principle of impedance-matching for underactuated wave energy harvesting systems. *Appl. Ocean Res.* **2021**, *118*, 102958. [CrossRef]

26. Padoan, A.; Scarciotti, G.; Astolfi, A. A Geometric Characterization of the Persistence of Excitation Condition for the Solutions of Autonomous Systems. *IEEE Trans. Autom. Control* **2017**, *62*, 5666–5677. [CrossRef]

27. Babarit, A.; Delhommeau, G. Theoretical and numerical aspects of the open source BEM solver NEMOH. In Proceedings of the 11th European Wave and Tidal Energy Conference, Nantes, France, 6–11 September 2015.

28. Faedo, N.; Peña-Sanchez, Y.; Ringwood, J.V. Finite-order hydrodynamic model determination for wave energy applications using moment-matching. *Ocean Eng.* **2018**, *163*, 251–263. [CrossRef]

29. Pena-Sanchez, Y.; Faedo, N.; Penalba, M.; Giuseppe, G.; Mérigaud, A.; Windt, C.; Violini, D.G.; LiGuo, W.; Ringwood, J. Finite-order hydrodynamic approximation by moment-matching (FOAMM) toolbox for wave energy applications. In Proceedings of the European Tidal and Wave Energy Conference Proceedings (EWTEC), Napoli, Italy, 1–6 September 2019; Volume 2019.

30. Khalil, H.K. *Nonlinear Systems*; Prentice-Hall: Upper Saddle River, NJ, USA, 1996.

31. Faedo, N.; Olaya, S.; Ringwood, J.V. Optimal control, MPC and MPC-like algorithms for wave energy systems: An overview. *IFAC J. Syst. Control* **2017**, *1*, 37–56. [CrossRef]

32. Isidori, A.; Astolfi, A. Disturbance attenuation and H_∞-control via measurement feedback in nonlinear systems. *IEEE Trans. Autom. Control* **1992**, *37*, 1283–1293. [CrossRef]